Elevated glucose levels favor SARS-CoV-2 infection and monocyte response through a HIF-1α/glycolysis dependent axis

Ana Campos Codo[1,16], Gustavo Gastão Davanzo[1,16], Lauar de Brito Monteiro[1,16], Gabriela Fabiano de Souza[2], Stéfanie Primon Muraro[2], Victor Corasolla Carregari[3], Carlos Alberto Oliveira de Biagi Junior[4], Fernanda Crunfli[3], Jeffersson Leandro Jimenez Restrepo[5], Pedro Henrique Vendramini[3], Guilherme Reis-de-Oliveira[3], Karina Bispo dos Santos[2], Daniel Augusto de Toledo Teixeira[2], Pierina Lorencini Parise[2], Matheus Cavalheiro Martini[2], Rafael Elias Marques Pereira Silva[6], Alexandre Borin[6], Laís Durço Coimbra[6], Vinícius O. Boldrini[2], Natalia S. Brunetti[2], Andre S. Vieira[7], Eli Mansour[8], Raisa G. Ulaf[8], Ana F. Bernardes[8], Thyago A. Nunes[8], Luciana C. Ribeiro[8], Andre Palma[8], Marcus V. Agrela[8], Maria Luiza Moretti[8], Helison R Carmo[9], Andrei C Sposito[9], Fabrício Bíscaro Pereira[10], Licio Augusto Velloso[8,11], Marco Aurélio Ramirez Vinolo[2,12], André Damasio[3,12], José Luiz Proença Módena[2], Robson Francisco Carvalho[13], Marcelo A. Mori[3,11,12], Daniel Martins-de-Souza[3,12,14,15], Helder I Nakaya[5], Alessandro S. Farias[2,12], Pedro Manoel M. Moraes-Vieira[1,11,12]*.

[1]Laboratory of Immunometabolism, Department of Genetics, Evolution, Microbiology and Immunology, Institute of Biology, Campinas State University, SP, Brazil.

[2]Department of Genetics, Evolution, Microbiology and Immunology, Institute of Biology, Campinas State University, SP, Brazil.

[3]Department of Biochemistry and Tissue Biology, Institute of Biology, Campinas State University, Campinas, SP, Brazil.

[4]Department of Genetics at Ribeirao Preto Medical School, University of Sao Paulo, Ribeirao Preto, SP, Brazil.

[5]Department of Clinical and Toxicological analyses, School of Pharmaceutical Sciences, University of Sao Paulo, Sao Paulo, SP, Brazil.

[6]Brazilian Biosciences National Laboratory (LNBio), Campinas, SP, Brazil.

[7]Department of Animal Biology, Institute of Biology, Campinas State University, Campinas, SP, Brazil.

[8]Department of Internal Medicine, School of Medical Sciences, University of Campinas, Campinas, SP, Brazil.

[9]Department of Clinical Medicine, School of Medical Sciences, University of Campinas, Campinas, SP, Brazil.

[10]Hematology and Hemotherapy Center, Campinas State University, Campinas, SP, Brazil.

[11]Obesity and Comorbidities Research Center (OCRC), University of Campinas, SP, Brazil.

[12]Experimental Medicine Research Cluster (EMRC), University of Campinas, SP, Brazil.

[13]Department of Structural and Functional Biology, Institute of Biosciences, Sao Paulo State University (UNESP), Botucatu, SP, Brazil.

[14]D'Or Institute for Research and Education (IDOR), SP, Brazil

[15]Instituto Nacional de Biomarcadores em Neuropsiquiatria, Conselho Nacional de Desenvolvimento Científico e Tecnologico, SP, Brazil.

[16]These authors contributed equally to this work.

*Corresponding Author and Lead Contact. E-mail: pmvieira@unicamp.br

HIGHLIGHTS

- Elevated glucose levels directly promote viral replication and cytokine expression.
- Aerobic glycolysis is necessary to sustain CoV-2 replication in monocytes and CoV-2-induced monocyte response.
- Mitochondrial ROS/HIF-1α axis is required for the induction of glycolysis and the consequent proinflammatory state of CoV-2-infected monocytes.
- Monocyte-derived cytokines drive T cell dysfunction and lung epithelial death.

SUMMARY

COVID-19 can result in severe lung injury. It remained to be determined why diabetic individuals with uncontrolled glucose levels are more prone to develop the severe form of COVID-19. The molecular mechanism underlying SARS-CoV-2 infection and what determines the onset of the cytokine storm found in severe COVID-19 patients are unknown. Monocytes/macrophages are the most enriched immune cell types in the lungs of COVID-19 patients and appear to have a central role in the pathogenicity of the disease. These cells adapt their metabolism upon infection and become highly glycolytic, which facilitates SARS-CoV-2 replication. The infection triggers mitochondrial ROS production, which induces stabilization of hypoxia-inducible factor-1α (HIF-1α) and consequently promotes glycolysis. HIF-1α-induced changes in monocyte metabolism by SARS-CoV-2 infection directly inhibit T cell response and reduce epithelial cell survival.

Targeting HIF-1α may have great therapeutic potential for the development of novel drugs to treat COVID-19.

INTRODUCTION

COVID-19 is a highly infectious disease caused by the acute respiratory syndrome coronavirus 2 (SARS-CoV-2). As of May 17, 2020, the pandemic of COVID-19 had already affected over 4 million people and taken over 300,000 lives (Organization, 2020; University, 2020). There is an urgent need for treatments and vaccines, however little is known about the cellular mechanisms that underlie SARS-CoV-2 (CoV-2) infection. The reasons why certain individuals are more prone to develop the severe form of COVID-19 are also elusive, although it is clear that age, cardiovascular diseases and diabetes are among the main risk factors for severe COVID-19 symptoms (Guo et al., 2020; Jordan et al., 2020; Zhou et al., 2020; Zhu et al., 2020). In a cohort of more than 7000 COVID-19 patients with or without diabetes, it was shown that uncontrolled blood glucose levels correlate with worse prognosis and higher mortality (Zhu et al., 2020). Dysregulated innate immune response with exaggerated inflammatory cytokine production are also a defining feature driving severe COVID-19 disease (Tay et al., 2020; Blanco-Melo et al., 2020). Myeloid cells, such as monocytes and macrophages are the most enriched immune cell types in the lungs of COVID-19 patients and may have a major role in the pathogenicity of the disease (Bost, 2020). The link between elevated glucose levels and uncontrolled inflammatory response in the lungs with the severity of COVID-19 disease prompted us to investigate the mechanism by which monocytes respond to SARS-CoV-2 infection in a context of elevated glucose supply.

RESULTS AND DISCUSSION

Once in the airway, CoV-2 infects host cells and starts to replicate. Upon infection, there is an accumulation of immune cells in the lungs, especially macrophages and monocytes (Merad and Martin, 2020). Using publicly available single-cell RNA-seq data from bronchoalveolar lavage (BAL) of mild and severe COVID-19 patients and controls (Bost, 2020), we identified that several genes associated with “interferon α/β signaling pathway” are up-regulated in mild and severe COVID-19 patients compared to controls in all 6 clusters of monocytes (Figure 1A). These monocytes are likely recruited by chemokines produced by infected epithelial cells, while interferons (IFN) induce angiotensin-converting enzyme 2 (ACE2), which allows other cells to be infected (Hoffmann et al., 2020; Wrapp et al., 2020). We showed that CoV-2 effectively infects peripheral blood monocytes and enhances the expression of angiotensin-converting enzyme 2 (ACE2) (Figure 1B-C), one of the proteins used by the virus to enter the cell (Hoffmann et al.,

2020; Wrapp et al., 2020). Monocytes infected with CoV-2 expressed higher levels of IFN α, β and λ, and higher levels of the proinflammatory cytokines TNF-α, IL-1β and IL-6, which are associated with the COVID-19 “cytokine storm” (Figure 1C).

Uncontrolled blood glucose levels observed in diabetic patients is a major risk factor for the severity of COVID-19 (Zhu et al., 2020). Thus, we hypothesized that glucose availability may affect viral replication capacity. We used increasing glucose concentrations to mimic human physiological and pathological conditions. Monocytes were cultured in low (2.5 mM), normal (5.5 mM), and high glucose conditions (11.1 mM and 22.2 mM). Glucose directly increased viral load, and ACE2 and IL-1β expression in CoV-2-infected monocytes in a dose-dependent manner (Figure 1D-F). Moreover, increased glucose levels further augmented TNF-α, IL-6, and IFN α, β and λ expression (Figure S1A). Altogether, these data indicate that elevated glucose levels directly promote viral replication and cytokine expression.

Once inside the cells, glucose can be oxidized by glycolysis to produce ATP and a number of other metabolites (Breda et al., 2019). We observed that several glycolysis-associated genes were up-regulated in BAL monocytes of COVID-19 patients (Figure 1A). Consistent with widespread metabolic remodeling, carbon metabolism pathways were enriched among the 144 differentially expressed proteins associated with energy metabolism in the proteomic analysis of CoV-2 infected monocytes cultured under 11.1 mM of glucose (used in all subsequent experiments unless stated otherwise). In total, 510 differentially expressed proteins were identified, playing roles in a range of biological processes (Figure S2A-C). In agreement with the metabolic remodeling observed in our proteomics study, CoV-2 stimulates glycolysis and increases the glycolytic capacity in monocytes (Figure 1G, Figure S1B). In summary, our results show that CoV-2 infection elicits a glycolytic profile in monocytes.

Next, we assessed the impact of CoV-2 infection on the cellular metabolism and function of monocytes. We used 2-deoxy-D-glucose (2-DG) to inhibit glucose flux and oligomycin to inhibit ATP synthase (Figure 2A). Treatment with 2-DG completely blocked the viral replication in CoV-2-infected monocytes, as well as the CoV-2 induced increase of ACE2 and IL-1β expression (Figure 2B-D). 2-DG treatment also inhibited CoV-2-induced TNF-α, IL-6, and IFN α, β and λ expression in monocytes (Figure S3A). In contrast, oligomycin treatment led to an increase in the viral load, ACE2 and IL-1β expression, as well as TNF-α, IL-6, α, β and λ IFN expression in monocytes (Figure 2E-G; Figure S3B). These data indicate that carbon flux through glycolysis, but not respiration coupled to ATP

synthesis, is necessary for CoV-2 replication and for CoV-2-induced monocyte immune response.

One glucose molecule yields two net ATP molecules through glycolysis. Galactose blunts aerobic glycolysis because galactose enters the glycolytic pathway at a lower rate (Leloir pathway) and yields no glycolytic derived ATP. This obligates the cell to rely exclusively on oxidative phosphorylation (OXPHOS) for ATP generation (Aguer et al., 2011; Buck et al., 2016). We infected human monocytes in glucose-free media and added either glucose, pyruvate or galactose as the main source of carbon for oxidation and subsequent ATP production. We observed that viral replication occurred when glucose or glucose + pyruvate were available and that the glucose + pyruvate effect was abolished in the presence of 2-DG (Figure 2H). When given only pyruvate or galactose, the virus was unable to replicate (Figure 2H). This indicates that CoV-2 replication requires the ATP generated specifically by glycolysis. Consistent with this notion, we inhibited pyruvate mitochondrial carrier with UK-5099 and determined that pyruvate-derived TCA cycle intermediates did not affect viral replication, and ACE2 and IL-1β expression in CoV-2-infected monocytes (Figure 2I; Figure S3C). These data suggest that the glycolytic flux is sufficient and necessary for CoV-2 replication. To reduce the glycolytic rate of monocytes, we inhibited the enzyme 6-phosphofructo-2-kinase/fructose-2,6-bisphosphatase-3 (PFKFB3), an allosteric activator of phosphofructokinase-1 (Breda et al., 2019) with 3-PO. This also resulted in decreased viral replication, and ACE2 and IL-1β expression (Figure 2J; Figure S3D). Finally, to evaluate the importance of aerobic glycolysis for CoV-2 infection, we blocked lactate dehydrogenase A (LDH-A) activity with oxamate. This also completely abrogated viral replication and reduced ACE2 and IL-1β expression in CoV-2 infected cells (Figure 2K; Figure S3E). Taken together, our results indicate that CoV-2 replication in monocytes and CoV-2-induced monocyte response are sustained by a switch to aerobic glycolysis (the Warburg effect).

When compared to healthy controls, BAL monocytes from severe COVID-19 patients had higher expression of HIF-1-target genes (Figure 3A). Our proteomic analysis further supports that CoV-2-infected monocytes have increased HIF-1α function given that HIF-1α targets are enriched among the up-regulated proteins (Figure 3B). HIF-1α is a strong inducer of glycolysis and IL-1β transcription (Tannahill et al., 2013). Blood monocytes from severe COVID-19 patients present high expression of HIF-1α in comparison to healthy donors (Figure 3C). We observed that HIF-1α protein levels and its transcriptional activity measured by the target genes GLUT-1, PFKFB3, PKM2 and LDH-A, which are involved in the glycolytic pathway, were increased in CoV-2-infected

monocytes (Figure 3D; Figure S4A). To determine the role of HIF-1α in CoV-2-mediated monocyte response, we treated cells with either the HIF-1α stabilizer BAY85-3934 or the HIF-1α inhibitor BAY87-2243. BAY87 decreased HIF-1α levels and completely abrogated CoV-2 replication (Figure 3E-F). HIF-1α inhibition also prevented the CoV-2 mediated increase in ACE2, IL-1β, TNF-α, IL-6, and IFN α, β and λ expression (Figure 3G-H; Figure S4B). Moreover, the expression of HIF-1α target genes was reduced upon BAY87 treatment in CoV-2-infected monocytes (Figure S4C). In contrast, HIF-1α stabilization in CoV-2-infected monocytes exacerbated the effects of CoV-2 infection, as shown by increased viral load and expression of ACE2, IL-1β, TNF-α, IL-6, and IFN α, β and λ, as well as higher HIF-1α transcriptional activity measured by an up-regulation of its target genes (Figure 3E-H; Figure S4B-C). Our findings demonstrated that HIF-1α is necessary for the induction of glycolysis and the consequent proinflammatory state of CoV-2-infected monocytes.

Next, we aimed to determine the mechanism by which CoV-2 increases HIF-1α levels and promotes a proinflammatory state. We observed that oxidative stress-associated genes are enriched in BAL of severe COVID-19 patients (Figure 3A). Reactive oxygen species (ROS) are strong inducers of HIF-1α (Mills et al., 2016). During metabolic reprogramming, the mitochondria is an important source of intracellular ROS (Mills et al., 2016). Proteomic analysis performed in CoV-2-infected monocytes confirms alterations on oxidative metabolism with an overall down-regulation of proteins involved in the TCA cycle (Figure S2D). In agreement, oxygen consumption was reduced in CoV-2-infected monocytes, which is known to increase mitochondrial ROS (mtROS) production (Mills et al., 2016) (Figure 3I). Consistently, we observed that CoV-2-infected monocytes have increased mtROS production as measured by mitoSOX (Figure 3J). Treatment of CoV-2-infected monocytes with antioxidants, such as mitoquinol (MitoQ) or thiol reductant N-Acetyl Cysteine (NAC) was sufficient to inhibit CoV-2-induced HIF-1α expression, viral replication, and increased expression of ACE2 and IL-1β in monocytes (Figure 3K-N). These antioxidants also prevent the up-regulation of TNF-α, IL-6, IFN α, β and λ and HIF-1α target genes (Figure S4D-E). Altogether, these results strongly highlight the metabolic alterations that take place in CoV-2-infected monocytes under high glucose conditions. These metabolic adaptations favor mtROS-induced HIF-1α stabilization to promote CoV-2 replication and monocyte inflammatory response.

Proinflammatory stimuli can negatively affect T cell response (de Marcken et al., 2019). The cytokines TNF-α, IL-1β and IL-6, which were highly expressed in CoV-2-infected monocytes (Figure 1C), resemble the cytokine storm proposed to take place in severe COVID-19 patients (Tay et al., 2020). The cytokine storm is thought to be associated

with lymphopenia in COVID-19 patients (Zheng et al., 2020). We tested whether immunometabolic reprogramming under high glucose concentrations during CoV-2 infection inhibits T cell proliferation. We co-cultured lymphocytes with allogeneic peripheral blood mononuclear cells in the presence of UV-inactivated conditioned media (CM) from mock (CM-mock) or CoV-2-infected monocytes treated with vehicle (CM-CoV-2), BAY87 (CM-BAY87) or MitoQ (CM-MitoQ). We found that CM-CoV-2 impaired CD4 and CD8 T cell proliferation (Figure 4A; Figure S4F), whereas CM-BAY87 or CM-MitoQ restored T cell proliferation to the same extent as CM-Mock (Figure 4A; Figure S4F). Because HIF-1α directly promotes IL-1β but not TNF-α and IL-6 expression (Tannahill et al., 2013), we tested whether IL-1β secretion affects T cell response. We observed that neutralization of IL-1β from UV-inactivated CM of CoV-2-infected monocytes with anti-IL-1β (CM-aIL-1β) restored T cell proliferation (Figure 4A; Figure S4F). The effect of CM-aIL-1β on T cell proliferation was similar to that observed with CM-BAY87 or CM-MitoQ (Figure 4A; Figure S4F). Published data showed that IFN-γ expression was reduced in CD4 T cells cocultured with RNA viruses-infected monocytes (de Marcken et al., 2019). Similarly, CM-CoV-2 decreased IFN-γ production by CD4 T cells and this was reversed in CM-BAY87 and CM-MitoQ and appear to be reversed in CM-aIL-1β (Figure 4B; Figure S4G). These results provide evidence to explain why elevated glucose levels during CoV-2 infection may lead to T cell dysfunction and lymphopenia.

Cytokine storm also plays a critical role in lung injury in patients with severe COVID-19 (Shi et al., 2020). However, whether this contributes to epithelial cell dysfunction is not clear. We treated the human pulmonary epithelial cell line A549 with CM-CoV-2 or CM-BAY87 and measured cell death. CM-CoV-2 induced apoptosis of A549 cells (Figure 4C), which was prevented when CoV-2-infected monocytes were treated with a HIF-1α inhibitor (Figure 4C). This suggests that under high glucose conditions CoV-2 infected monocytes can promote epithelial cell death in a mtROS/HIF-1α dependent manner.

In conclusion, we showed that CoV-2-infected monocytes express large amounts of proinflammatory cytokines and IFNs. Elevated glucose levels directly induce viral replication and proinflammatory cytokine expression. Glycolysis-derived ATP and glycolytic flux are required for CoV-2 replication. CoV-2-induced mtROS production stabilizes HIF-1α, which in turn upregulates glycolytic genes and IL-1β expression. Finally, we demonstrate that CoV-2 infected monocytes promote T cell dysfunction and lung epithelial cell death. These data may explain why uncontrolled diabetes may lead to compromised adaptive immune response and lung dysfunction in patients with severe COVID-19 symptoms. Our results also provide mechanistic evidence to suggest that the mtROS/HIF-1α/glycolysis-axis could be targeted to treat COVID-19 disease.

ACKNOWLEDGMENTS

We thank the Hematology and Hemotherapy Center of Unicamp (Campinas, SP - Brazil), Nelson Cabral Junior and Regina Amelia Moraes for providing the buffy coats used for PBMC isolation in this study. We thank Elzira E. Saviani for technical support. We would like to thank Aline Mika Matsuguma for designing our schematic figures. We gratefully acknowledge Dr. Catherine A. Reardon from the Committee on Molecular Metabolism and Nutrition, University of Chicago and from Ben May Department for Cancer Research, University of Chicago, Chicago, IL, USA for the manuscript editing. We thank the Sao Paulo Research Foundation - FAPESP (grant numbers 2015/15626-8, 2016/23328-0, 2016/18031-8, 2017/22669-0, 2018/22505-0, 20/04579-7, 2020/04746-0, 2019/06372-3, 2020/04558-0, 2020/04919-2, 2020/04583-4, 2017/01184-9, 2020/04522-5, 2017/01184-9, 2017/255881-1, 2020/04746-0, 2019/00098-7), Fundo de Apoio ao Ensino, Pesquisa e Extensão (FAEPEX) Unicamp - Grant number: 2274/20, the Brazilian National Council for Scientific and Technological Development - CNPq, and the Coordenação de Aperfeiçoamento de Pessoal de Nível Superior – Brazil (CAPES) – Finance Code 001 for funding this project.

AUTHOR CONTRIBUTIONS

Conceptualization: Codo AC, Davanzo GG, Monteiro LB, Moraes-Vieira PM, Farias AS. Methodology: Codo AC, Davanzo GG, Monteiro LB, Moraes-Vieira PM, Farias AS. Software: Nakaya HI, Carvalho RF, Biagi-Junior CAO, Jimenez L, Martins-de-Souza D, Carregari VC, Crunfli F, Vendramini PH, Reis-de-Oliveira G. Validation: Vieira AS. Formal analysis: Codo AC, Davanzo GG, Farias AS, Martins-de-Souza D, Carvalho RF, Nakaya HI. Investigation: Codo AC, Davanzo GG, Monteiro LB, Farias AS, de Souza GF, Muraro SP, Martini MC, Parise PL, Toledo-Teixeira DA, Bispo-dos-Santos K, Marques RE, Coimbra LD, Borin A, Boldrini VO, Brunetti NS, Martins-de-Souza D, Carregari VC, Crunfli F, Vendramini PH, Reis-de-Oliveira G. Farias AS, Mansour E, Ulaf RG, Bernardes AF, Nunes TA, Ribeiro LC, Palma A, Agrela MV, Moretti ML. Resources: Moraes-Vieira PM, Mori MA, Proença-Modena JL, Vinolo MAR, Velloso LA. Data curation: Codo AC, Davanzo GG, Monteiro LB, Moraes-Vieira PMM, Farias AS, Martins-de-Souza D, Nakaya HI, Carvalho RF. Writing - original draft: Codo AC, Davanzo GG, Monteiro LB., Moraes-Vieira PM. Writing - Review and editing: Codo AC, Davanzo GG, Monteiro LB, Nakaya HI, Damasio A, Farias AS, Pronça-Modena JL, Mori MA, Vinolo MAR, Moraes-Vieira PM. Visualization: Codo AC, Davanzo GG, Monteiro LB, Farias AS. Supervision: Moraes-Vieira PM. Project administration: Codo AC, Davanzo GG, Monteiro LB, Moraes-Vieira PM.

DECLARATION OF INTERESTS

Authors declare no competing interests.

REFERENCES

Aguer, C., Gambarotta, D., Mailloux, R.J., Moffat, C., Dent, R., McPherson, R., and Harper, M.E. (2011). Galactose enhances oxidative metabolism and reveals mitochondrial dysfunction in human primary muscle cells. PLoS One *6*, e28536.

Blanco-Melo, D., Nilsson-Payant, B.E., Liu, W-C., Uhl, S., Hoagland, D., Møller, R., Jordan, T.X., Oishi, K., Panis, M., Sachs, D., Wang, T.T., Schwartz, R.E., Lim, J.K., Albrecht, R.A., tenOever, B.R. (2020). Imbalanced Host Response to SARS-CoV-2 Drives Development of COVID-19. Cell.

Bost, P., Giladi, A., Liu, Y., Bendjelal, Y., Xu, G., David, E., Blecher-Gonen, R., Cohen, M., Medaglia, C., Li, H., Deczkowska, A., Zhang, S., Schwikowski, B., Zhang, Z., Amit, I. (2020). Host-viral infection maps reveal signatures of severe COVID-19 patients. Cell.

Breda, C.N.S., Davanzo, G.G., Basso, P.J., Saraiva Camara, N.O., and Moraes-Vieira, P.M.M. (2019). Mitochondria as central hub of the immune system. Redox Biol *26*, 101255.

Buck, M.D., O'Sullivan, D., Klein Geltink, R.I., Curtis, J.D., Chang, C.H., Sanin, D.E., Qiu, J., Kretz, O., Braas, D., van der Windt, G.J., et al. (2016). Mitochondrial Dynamics Controls T Cell Fate through Metabolic Programming. Cell *166*, 63-76.

Chen, E.Y., Tan, C.M., Kou, Y., Duan, Q., Wang, Z., Meirelles, G.V., Clark, N.R., and Ma'ayan, A. (2013). Enrichr: interactive and collaborative HTML5 gene list enrichment analysis tool. BMC Bioinformatics *14*, 128.

de Marcken, M., Dhaliwal, K., Danielsen, A.C., Gautron, A.S., and Dominguez-Villar, M. (2019). TLR7 and TLR8 activate distinct pathways in monocytes during RNA virus infection. Sci Signal *12*.

Guo, W., Li, M., Dong, Y., Zhou, H., Zhang, Z., Tian, C., Qin, R., Wang, H., Shen, Y., Du, K., et al. (2020). Diabetes is a risk factor for the progression and prognosis of COVID-19. Diabetes Metab Res Rev, e3319.

Hoffmann, M., Kleine-Weber, H., Schroeder, S., Kruger, N., Herrler, T., Erichsen, S., Schiergens, T.S., Herrler, G., Wu, N.H., Nitsche, A., et al. (2020). SARS-CoV-2 Cell Entry Depends on ACE2 and TMPRSS2 and Is Blocked by a Clinically Proven Protease Inhibitor. Cell *181*, 271-280 e278.

Jordan, R.E., Adab, P., and Cheng, K.K. (2020). Covid-19: risk factors for severe disease and death. BMJ *368*, m1198.

Medeiros, A.I., Bonato, V.L., Malheiro, A., Dias, A.R., Silva, C.L., and Faccioli, L.H. (2002). Histoplasma capsulatum inhibits apoptosis and Mac-1 expression in leucocytes. Scand J Immunol *56*, 392-398.

Merad, M., and Martin, J.C. (2020). Pathological inflammation in patients with COVID-19: a key role for monocytes and macrophages. Nat Rev Immunol.

Mills, E.L., Kelly, B., Logan, A., Costa, A.S.H., Varma, M., Bryant, C.E., Tourlomousis, P., Dabritz, J.H.M., Gottlieb, E., Latorre, I., et al. (2016). Succinate Dehydrogenase Supports Metabolic Repurposing of Mitochondria to Drive Inflammatory Macrophages. Cell *167*, 457-470 e413.

Organization, W.H. (2020).

Otasek, D., Morris, J.H., Boucas, J., Pico, A.R., and Demchak, B. (2019). Cytoscape Automation: empowering workflow-based network analysis. Genome Biol *20*, 185.

Shannon, P., Markiel, A., Ozier, O., Baliga, N.S., Wang, J.T., Ramage, D., Amin, N., Schwikowski, B., and Ideker, T. (2003). Cytoscape: a software environment for integrated models of biomolecular interaction networks. Genome Res *13*, 2498-2504.

Shi, Y., Wang, Y., Shao, C., Huang, J., Gan, J., Huang, X., Bucci, E., Piacentini, M., Ippolito, G., and Melino, G. (2020). COVID-19 infection: the perspectives on immune responses. Cell Death Differ *27*, 1451-1454.
Simko, T.W.a.V. (2017). R package "corrplot": Visualization of a Correlation Matrix (Version 0.84).
Tannahill, G.M., Curtis, A.M., Adamik, J., Palsson-McDermott, E.M., McGettrick, A.F., Goel, G., Frezza, C., Bernard, N.J., Kelly, B., Foley, N.H., et al. (2013). Succinate is an inflammatory signal that induces IL-1beta through HIF-1alpha. Nature *496*, 238-242.
Tay, M.Z., Poh, C.M., Renia, L., MacAry, P.A., and Ng, L.F.P. (2020). The trinity of COVID-19: immunity, inflammation and intervention. Nat Rev Immunol.
University, J.H. (2020).
Wang, Y., Dong, C., Hu, Y., Li, C., Ren, Q., Zhang, X., Shi, H., and Zhou, M. (2020). Temporal Changes of CT Findings in 90 Patients with COVID-19 Pneumonia: A Longitudinal Study. Radiology, 200843.
Won, J., Lee, S., Park, M., Kim, T.Y., Park, M.G., Choi, B.Y., Kim, D., Chang, H., Kim, V.N., and Lee, C.J. (2020). Development of a Laboratory-safe and Low-cost Detection Protocol for SARS-CoV-2 of the Coronavirus Disease 2019 (COVID-19). Exp Neurobiol.
Wrapp, D., Wang, N., Corbett, K.S., Goldsmith, J.A., Hsieh, C.L., Abiona, O., Graham, B.S., and McLellan, J.S. (2020). Cryo-EM structure of the 2019-nCoV spike in the prefusion conformation. Science *367*, 1260-1263.
Yu, G., Wang, L.G., Han, Y., and He, Q.Y. (2012). clusterProfiler: an R package for comparing biological themes among gene clusters. OMICS *16*, 284-287.
Zheng, M., Gao, Y., Wang, G., Song, G., Liu, S., Sun, D., Xu, Y., and Tian, Z. (2020). Functional exhaustion of antiviral lymphocytes in COVID-19 patients. Cell Mol Immunol *17*, 533-535.
Zhou, F., Yu, T., Du, R., Fan, G., Liu, Y., Liu, Z., Xiang, J., Wang, Y., Song, B., Gu, X., et al. (2020). Clinical course and risk factors for mortality of adult inpatients with COVID-19 in Wuhan, China: a retrospective cohort study. Lancet *395*, 1054-1062.
Zhou, G., Soufan, O., Ewald, J., Hancock, R.E.W., Basu, N., and Xia, J. (2019). NetworkAnalyst 3.0: a visual analytics platform for comprehensive gene expression profiling and meta-analysis. Nucleic Acids Res *47*, W234-W241.
Zhu, L., She, Z.G., Cheng, X., Qin, J.J., Zhang, X.J., Cai, J., Lei, F., Wang, H., Xie, J., Wang, W., et al. (2020). Association of Blood Glucose Control and Outcomes in Patients with COVID-19 and Pre-existing Type 2 Diabetes. Cell Metab.

STAR+METHODS

KEY RESOURCES TABLE

REAGENT	SOURCE	IDENTIFIER
Antibodies		
anti-CD14-FITC (clone M5E2)	BD Biosciences	Cat#555397
anti-HIF-1α-PE (clone 241812)	R&D Systems	Cat.IC1935P
anti-IFN-γ-PECy7 (clone B27)	BD Biosciences	Cat#557643
anti-CD4-APC (clone RPA-T4)	BD Biosciences	Cat#555349
anti-CD3-PERCPCy5.5 (clone SP34-2)	BD Biosciences	Cat#552852
anti-CD8-APCCy7 (clone SK1)	BD Biosciences	Cat#557834
Chemicals		
FICOLLl® - PAQUE PLUS	Sigma-Aldrich	Cat.GE17-1440-03
RPMI 1640	Thermo Fisher Scientific	Cat#11875119
Penicillin-Streptomycin	Sigma-Aldrich	Cat.P4333
Minimum Essential Medium (MEM)	Sigma-Aldrich	Cat. M0325
Fetal Bovine Serum (FBS)	Thermo Fisher Scientific	Cat#12657029
Dulbecco's Modified Eagle Medium (DMEM)	Thermo Fisher Scientific	Cat#11885084
2-DG	Cayman Chemicals	Cat#14325
3-PO	Cayman Chemicals	Cat#19276
UK-5099	Cayman Chemicals	Cat#16980
Oligomycin D	Cayman Chemicals	Cat#20184
BAY 85-3934	Cayman Chemicals	Cat#15297
MitoQ	Cayman Chemicals	Cat#89950
N-acetyl-L-Cysteine	Cayman Chemicals	Cat#20261
Oxamate	Biocompare	Cat#2580
BAY 87-2243	Selleckchem	Cat.S7309
TRIzol Reagent	Sigma-Aldrich	Cat.T9424
BD Horizon™ Fixable Viability Stain 510	BD Biosciences	Cat#564406
MitoSOX Red Mitochondrial Superoxide Indicator	Thermo Fisher Scientific	Cat.M36008
phorbol 12-myristate 13-acetate (PMA)	Sigma-Aldrich	Cat. P1585
calcium ionophore (A23187)	Sigma-Aldrich	Cat. C7522
Brefeldin A	BioLegend	Cat#420601
p-formaldehyde	Sigma-Aldrich	Cat.F1635

carboxyfluorescein succinimidyl ester (CellTrace™ CFSE)	BioLegend	Cat#423801
Critical Commercial Assays		
GoScript™ Reverse Transcriptase cDNA synthesis kit	Promega	Cat. A2791
SybrGreen Supermix	Qiagen	Cat. 208156
Bradford assay	Bio-Rad	
Cell lines		
Vero CCL-81	ATCC	ATCC CCL-81
A549 CCL-185	ATCC	ATCC CCL-185
Software and Algorithms		
Prism8	GaphPad	N/A
FlowJo software	BD Biosciences	N/A

CONTACT FOR REAGENT AND RESOURCE SHARING

Further information and requests for reagents may be directed to and will be fulfilled by the Lead Contact, Pedro Manoel M. Moraes-Vieira (pmvieira@unicamp.br).

EXPERIMENTAL MODEL AND SUBJECT DETAILS

Sample acquisition from COVID-19 patients

Human blood samples from severe COVID-19 patients analyzed in this study were obtained from individuals admitted at the Clinics Hospital, University of Campinas and included in a clinical trial (UTN: U1111-1250-1843). All samples were collected before intervention. SARS-CoV-2 infection was diagnosed using real-time PCR and severe COVID-19 was defined by the presence of typical lung CT-scan images and low resting blood O2 saturation. Lung CT-scans were analyzed by two lung-specialized radiologists and ranked according to a previous publication (Wang et al., 2020). Parameters of COVID-19 patients analyzed in this study are described on Table S1. All study was approved by the Brazilian Committee for Ethics in Human Studies (CAEE: 30227920.9.0000.5404).

PBMCs isolation

Peripheral blood from healthy donors was obtained from buffy coats provided by Unicamp's Hematology and Hemotherapy Center (SP-Campinas, Brazil). Peripheral blood mononuclear cells (PBMCs) were isolated by density-gradient centrifugation using 1.077 g × mL−1 Ficoll gradient. Briefly, buffy coats were gently mixed and then diluted

(1:1) with Phosphate Buffer Saline (PBS) and carefully transferred to 50-mL tube containing 10 mL of Ficoll, which was centrifuged at 2700 rpm for 20 min at room temperature. Total PBMCs were cultured as adherent monolayers (1,5 × 106 cell × mL−1) in RPMI 1640. After 2-3 h of adhesion, cells were washed with PBS and incubated overnight with RPMI 1640 containing 10% FBS and 1% Penicillin-Streptomycin incubated at 37°C with 5% CO2 atmosphere.

METHOD DETAILS

Virus and cell lines

HIAE-02 SARS-CoV-2/SP02/human/2020/BRA (GenBank accession number MT126808.1) virus was isolated from the first confirmed case in Brazil and kindly donated by Professor Dr. Edson Luiz Durigon. All Sars-CoV-2 virus stocks were propagated in the Vero cell line and supernatant was harvested at 2–3 dpi. The viral titers were determined by plaque assays on Vero cells. Vero CCL-81 cells were cultivated in MEM supplemented with 10% heat inactivated fetal bovine serum (FBS) and 1% Penicillin-Streptomycin, and incubated at 37°C with 5% CO2 atmosphere. A549 cell line were cultivated in DMEM supplemented with 10% FBS and 1% Penicillin-Streptomycin and incubated at 37°C with 5% CO2 atmosphere.

Reagents and infection

PBMCs were treated with inhibitors for 2 h prior to viral infection. Cells were infected with SARS-CoV-2 at MOI 0.1 under continuous agitation at 15 rpm for 1 h for virus absorption. After infection, cells were washed with pre-warmed PBS twice and incubated in RPMI containing 10% FBS and 1% Penicillin-Streptomycin for 24h at 37°C with 5% CO2 atmosphere.

RNA extraction, viral load and gene expression analyses

Total RNA extractions were performed using TRIzol Reagent according to manufacturer's instructions. RNA concentration was determined by NanoDrop 2000 spectrophotometer (Thermo Scientific). Extracted total RNA was reverse-transcribed using GoScript™ Reverse Transcriptase cDNA synthesis kit according to the manufacturer's instructions. For viral load detection, specific SARS-CoV-2 N1 primers targeting the N1 region were used as previously described (Won et al., 2020). Standard curve was generated using serial dilutions of SARS-CoV-2. Viral load and gene expression qRT-PCR were performed using SybrGreen Supermix. All qRT-PCR reactions were performed using BIO-RAD CFX394 Touch Real-Time PCR Detection System on 384-well plates. Gene expression fold change was calculated with the ΔΔCt

method using Microsoft Excel. Briefly, ΔΔCt = ΔCt(SARS-CoV-2-infected) –ΔCt(mock control) with ΔCt = Ct(gene-of-interest) – Ct(housekeeping-gene-18S). The fold change for each gene is calculated as 2^-ΔΔCt. The sequences of the primers used are available in Table S2.

Real-time metabolic assays

An XFe24 Extracellular Flux analyzer (Agilent) was used to determine the bioenergetic profile of PBMCs. PBMCs were plated at 4,000,000 cells per well in XFe24 plates 3 h before infection with SARS-CoV-2. Glycolytic Stress and Mito Stress Tests were performed on XFe24 Bioanalyzer at 24 h post infection, all assays were performed following manufacturer's protocols. Results were normalized to cell number.

mtROS production

After 24 h post infection, PBMCs were collected and stained with BD Horizon™ Fixable Viability Stain 510, MitoSOX Red Mitochondrial Superoxide Indicator and anti-CD14-FITC for 15 min at 37ºC. Cells were washed with PBS, fixed with 4% p-formaldehyde for 30 min at 4°C and transferred to polypropylene FACS tubes. Cells were then analyzed using a FACSVerse™ (Becton & Dickinson, San Diego, CA, USA) flow cytometer, and data were analyzed using FlowJo software.

HIF-1α staining

After 24 h post infection, PBMCs were fixed with 4% p-formaldehyde for 30 min at 4°C. Cells were washed with PBS, permeabilized, and incubated with anti-CD14-FITC and anti-HIF-1α-PE for 1 h at 4° C. Cells were then acquired by flow cytometry (FACSVerse™ – Becton & Dickinson, San Diego, CA, USA) and analyzed using FlowJo software.

Generation of conditioned medium

Conditioned medium was generated by incubating PBMCs with mock control or SARS-CoV-2 as described previously. Supernatant from each condition was collected and placed under UV light for 30 min for residual virus inactivation. Supernatants were stored in -80°C until used in human T cell and epithelial cell assays.

Human lymphocyte isolation and mixed lymphocyte reaction

PBMCs isolated from buffy coats from healthy volunteers were incubated at 37°C and 5% CO2 for 2 h to allow monocytes adherence to the plate surface. Non-adherent cells in suspension were collected and stained with carboxyfluorescein succinimidyl ester (CellTrace™ CFSE). Briefly, cells were incubated with CFSE diluted in pre-warmed PBS to the desired concentrations at 37° for 15 min and then resuspended in a fresh pre-

warmed medium for another 30 min and then washed with PBS, according to the manufacturer's recommendation. 5 × 10^5 lymphocytes were cocultured with 5 × 10^4 allogeneic PBMCs in the presence of different conditioned medium for 72h. After 72h, cells were stimulated with 0.1 µg × mL−1 phorbol 12-myristate 13-acetate (PMA) and 0.5 µg × mL−1 calcium ionophore (A23187) in the presence of brefeldin A (10 µg × mL−1) for 4 h, labeled with fixable viability stain, permeabilized, and incubated with anti-IFN-γ-PECy7, anti-CD4-APC, anti-CD3-PERCPCy5.5 and anti-CD8-APCCy7. Cells were then acquired by flow cytometry (FACSymphony – Becton & Dickinson, San Diego, CA, USA) and analyzed using FlowJo software.

Epithelium apoptosis assay

Epithelial cells from cell line A549 were incubated in the presence of different conditioned medium for 24 h. The percentage of live (AnnexinV-/PI-), early (AnnexinV+/PI-) and late (AnnexinV+/PI+) apoptotic cells was determined by flow cytometry (FACSVerse™ – Becton & Dickinson, San Diego, CA, USA) after labeling with Annexin V/PI, as previously described (Medeiros et al., 2002).

Proteomics Sample Preparation, Mass Spectrometry, and Data Processing

Macrophages and monocytes isolated from 5 healthy controls were chemically (Lysis Buffer: 100 mM TrisHCL, 1 mM EDTA, 150 mM NaCL, 1% triton-x, protease and phosphatase inhibitors), and mechanically lysed (Ultrasonication probe) then the total protein extract was quantified by Bradford assay, according to manufacturer's instruction (Bio-Rad). Aliquots of 60 µg of total protein extract were transferred on Microcon-10 Centrifugal Filter, with 10 kDa cut off, for filter-aided sample preparation (FASP) protein digestion, as described (Distler, U., et al 2016). Proteins were reduced by 10 mM (dithiothreitol) DTT and alchilated by 50 mM iodoacetamide (IAA). Each protein aliquot was digested over-night by trypsin. In detail, trypsin digestions were carried out at 37°C, 16-18 h in 50 mM ammonium bicarbonate (AMBIC) pH=8.0. The day after, all digestions were blocked by adding formic acid (FA) to a final concentration of 0.5% (v/v) and the peptides were recovered from the filter in 50 mM AMBIC, concentrated in a speedvac and stored at -80°C until use.

Digested peptides from each sample were resuspended in 0.1% FA. The separation of tryptic peptides was performed on an ACQUITY MClass System (Waters Corporation). 0.50µg of each digested sample was loaded onto a Symmetry C18 5 µm, 180 µm × 20 mm precolumn (Waters Corp.) used as trapping column and subsequently separated by a 120 min reversed phase gradient at 300 nL × min-1 (linear gradient, 3–55% ACN over 90 min) using a HSS T3 C18 1.8 µm, 75 µm × 150 mm nanoscale and LC column (Waters

Corp.) maintained at 40°C. For the gradient elution water-Formic Acid (99.9/0.1, v/v) was used as eluent A and Acetonitrile Formic Acid (99.9/0.1, v/v) as eluent B. The Separated peptides have been analyzed by High Definition Synapt G2-Si Mass spectrometer directly coupled to the chromatographic system. Differential protein expression was evaluated with a data-independent acquisition (DIA) of shotgun proteomics analysis by Expression configuration mode (MSe). The mass spectrometer operated in “Expression Mode” switching between low (4 eV) and high (25–60 eV) collision energies on the gas cell, using a scan time of 1.0s per function over 50–2000 m/z. All spectra were acquired in Ion Mobility Mode by applying a wave velocity for the ion separation of 1.000m/s and a transfer wave velocity of 175 m/s. The processing of low and elevated energy, added to the data of the reference lock mass ([Glu1]-Fibrinopeptide B Standard, Waters Corp.) provides a time-aligned inventory of accurate mass retention time components for both the low and elevated-energy (EMRT, exact mass retention time) Each sample was run in three technical replicates.

Continuum LC-MS data from three replicate experiments for each sample were processed for qualitative and quantitative analysis using the software Progenesis (Waters Corp.). The qualitative identification of proteins was obtained by searching in Homo Sapiens database (UNIPROT Protein reviewed release 2020-04). Search parameters were set as: automatic tolerance for precursor ions and for product ions, minimum 2 fragment ions matched per peptide, minimum 3 fragment ions matched per protein, minimum 1 peptide matched per protein, 2 missed cleavage, carbamydomethylation of cysteines as fixed modification and oxidation of methionines as variable modifications, false discovery rate (FDR) of the identification algorithm < 1%.

Label free quantitative analysis was obtained using the relative abundance intensity integrated in Progenesis software, using all peptides identified for normalization. The expression analysis was performed considering technical replicates available for each experimental condition following the hypothesis that each group is an independent variable. Filtered tables were generated to include proteins found at least in two out of three technical replicates and to exclude proteins showing less than 20% change and those showing no statistical significance according to ANOVA ≥ 0.05.

Protein ontologies and network analysis

To identify biologically relevant molecular pathways, the proteomic dataset was analyzed by a bioinformatic analysis tool based on QIAGEN’S Ingenuity Pathways Analysis (QIAGEN’S Ingenuity pathway analysis, Ingenuity Systems, http://www.qiagen.com /ingenuity). This allows us to explore functional associations relevant to the experimental

results. The analysis parameters were set as: Direct and indirect relationship; endogenous chemical substances included; all molecules and/or relationships considered as Summary Filter. The most significant categories associated with the loaded datasets were identified by calculating their significance (p-value, Fischer test). A p-value threshold of 0.05 has been set as significant for an association between gene/proteins present in the data sets and each pathway (Canonical pathway, Upstream regulators and Biological Function). For the Gene Ontology analysis, we made use of the PANTHER 14.0 (Protein ANalysis THrough Evolutionary Relationships) Classification System (GENEONTOLOGY Unifying Biology) containing 15.552 protein families, and STRING: functional protein association networks, v.11.0.

The heatmap was built with the heatmapper (http://www.heatmapper.ca/expression), using the median value of the 3 normalized log2 technical replicates of the sum of the Intensity Peaks for each protein identified in each patient. We used an Average Linkage clustering method and the Pearson correlation method for the measurement of the linear correlation between variable samples.

The visualization of proteomic data was performed in the Python programming language (v. 3.7.3). The pathway enrichment analyses were carried out in ClusterProfiler (Yu et al., 2012) and were visualized in R (v. 4.0) (5) and Cytoscape environments (v. 3.8) (Otasek et al., 2019; Shannon et al., 2003).

Re-analysis of scRNA-seq Data

The scRNA-seq data from bronchoalveolar lavage fluid (BALF) from patients with varying severity of COVID-19 disease and from healthy was acquired from the Gene Expression Omnibus (GEO) database under the series number GSE145926, which contains 12 data of lung tissue generated using 3' V2 chemistry kit on Chromium Single cell controller (10xGenomics). Filtered feature-barcode matrix was used in the following analysis. All additional analysis was performed using Seurat v3. Cells with less than 200 genes detected or greater than 10% mitochondrial RNA content were excluded from analysis, with 90,046/94,583 cells passing filter (95%).

For clustering of all cell types in the BALF of patients, raw UMI counts were log normalized and variable genes called on each dataset independently based on average expression greater than 0.1 and average dispersion greater than 1. To remove batch effects between samples associated with a housekeeping gene expression signature, we assigned a housekeeping score using the AddModuleScore function based on C1orf43 CHMP2A, EMC7, GPI, PSMB2, PSMB4, RAB7A, REEP5, SNRPD3, VCP, VPS29 genes. Additionally, we assigned scores for S and G2/M cell cycle phases based

on previously defined gene sets using the CellCycleScoring function. Scaled z-scores for each gene were calculated using the ScaleData function and regressed against the number of UMIs per cell, mitochondrial RNA content, S phase score, G2/M phase score and housekeeping score. Scaled data was used as an input into PCA based on variable genes. Clusters were identified using shared nearest neighbor (SNN) based clustering based on the first 20 PCs with k = 30 and resolution = 0.4. The same principal components were used to generate the UMAP projections, which were generated with a minimum distance of 1 and 20 neighbors.

Differentially expressed genes between mild/severe COVID-19 patients and controls for each cluster were identified using FDR < 0.05 and |avg_logFC| > 0.25. Functional enrichment analysis was performed using Enrichr tool (Chen et al., 2013). As input, we utilized the genes that were up-regulated in mild/severe COVID-19 patients compared to controls in each one of the 6 CD14+ monocyte clusters. Corrplot R package (Simko, 2017) was used to display the enrichment score.

Network analysis was performed with NetworkAnalyst tool (Zhou et al., 2019). As input, we utilized the genes that were up-rgulated in severe COVID-19 patients compared to controls in at least 3 out 6 CD14+ monocyte clusters (parameters: IMEx Interactome as protein-protein interaction and Minimum Network). Data was visualized by Cytoscape tool (Shannon et al., 2003).

Statistical analysis

Proteomic and RNA-seq were analyzed as described above. Additional data were plotted and analyzed using the GraphPad Prism 8.0 software (GraphPad Software, San Diego, CA). For analyses between 2 groups, Student's t test was used. For comparisons among more than 2 groups, either one-way ANOVA, followed by Tukey post hoc tests was used. Differences were considered statistically significant when P value was <0.05.

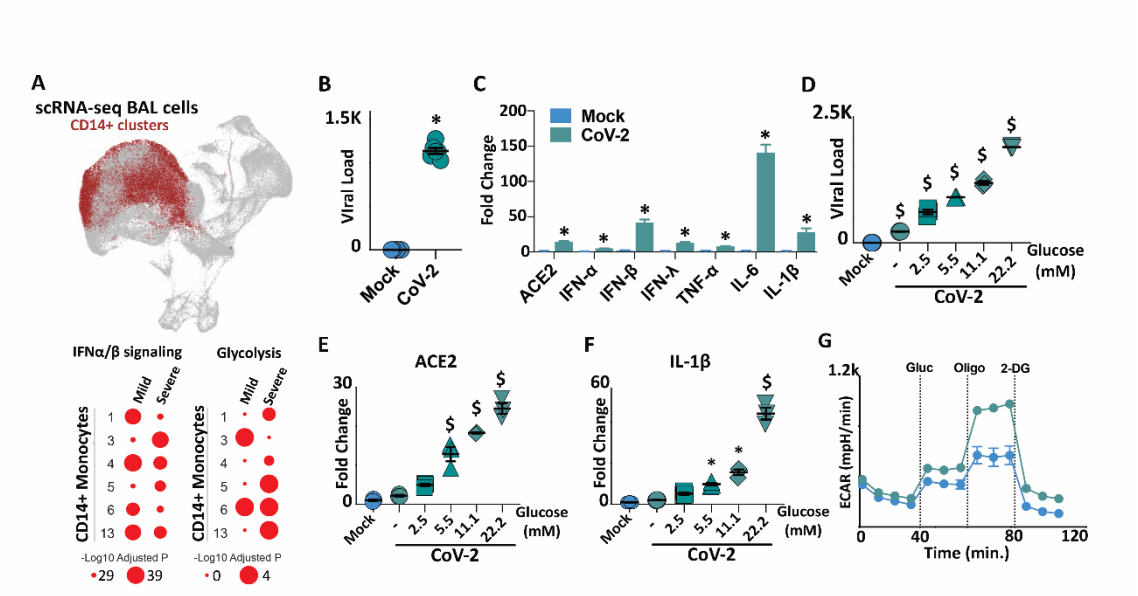

Figure 1. SARS-CoV-2 infection induces glycolysis in human monocytes.

(A) Single-cell RNAseq data showing CD14+ monocyte clusters expressing IFN-α and IFN-β in both mild and severe COVID-19 patients compared to healthy individuals. Enrichment of glycolysis in monocytes of severe COVID-19 patients.

(B-C) Human monocytes were infected with mock control or SARS-CoV-2 (CoV-2) (MOI 0.1) for 1 h under continuous agitation and incubated for 24 h. (B) CoV-2 viral load in human monocytes. (C) Relative mRNA expression of ACE2, IFN-α, IFN-β, IFN-λ, TNF-α, IL-6 and IL-1β by qPCR.

(D-F) Human monocytes were infected with mock control or CoV-2 (MOI 0.1) for 1h under continuous agitation and rest for 24 h in media containing different glucose concentrations (0, 2.5, 5.5, 11.1 and 22.2 mM). (D) Analysis of viral load by qPCR. Relative mRNA expression of (E) ACE2 and (F) IL-1β.

(G) Extracellular Acidification Rate (ECAR) of human monocytes upon glycolytic stress (following injections of Glucose, Oligomycin and 2-DG) after 24 h post-infection.

Data represent mean ± SEM of at least three independent experiments performed in triplicate. *P < 0.05 compared to mock. $P < 0.05 compared to all other groups. (One-Way ANOVA and Tukey post hoc tests).

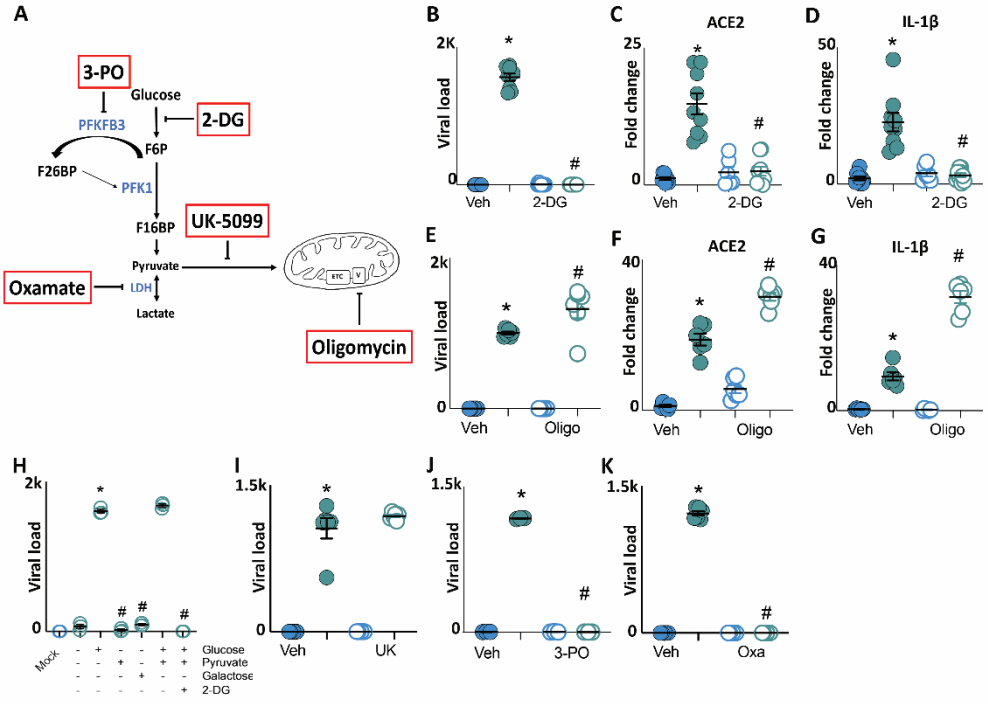

Figure 2. Glycolysis sustains SARS-CoV-2 replication in human monocytes.

Human monocytes were pre-treated for 2 h with metabolic modulators (PFKFB3 inhibitor 3-PO, glycolysis inhibitor 2-DG, mitochondrial pyruvate carrier inhibitor UK-5099 (UK), LDH-A inhibitor oxamate (OXA), ATP synthase inhibitor oligomycin (Oligo)) prior to SARS-CoV-2 (CoV-2) infection (MOI 0.1) for 1 h under continuous agitation and incubation for 24 h.

(A) Schematic of metabolism modulators mechanism of action.

(B) Viral load by qPCR of infected monocytes pre-treated with 2-DG.

(C-D) Relative mRNA expression of (C) ACE2 and (D) of IL-1β in infected monocytes pre-treated with 2-DG by qPCR.

(E) Viral load by qPCR of infected monocytes pre-treated with Oligo.

(F-G) Relative mRNA expression of (F) ACE2 and (G) IL-1β in monocytes treated with Oligo.

(H) Human monocytes were given either glucose, pyruvate or galactose as a carbon source for ATP. 2-DG was used as a glucose metabolism inhibitor. These cells were infected for 1 h with CoV-2 (MOI 0.1), followed incubation for 3 h and viral load was analyzed by qPCR.

(I-K) Viral load in CoV-2-infected monocytes treated with (I) UK, (J) 3-PO and (K) OXA by qPCR.

All data represent mean ± SEM of at least three independent experiments performed in triplicate. *P < 0.05 compared to mock. #P < 0.05 compared to CoV-2 (One-Way ANOVA and Tukey post hoc tests).

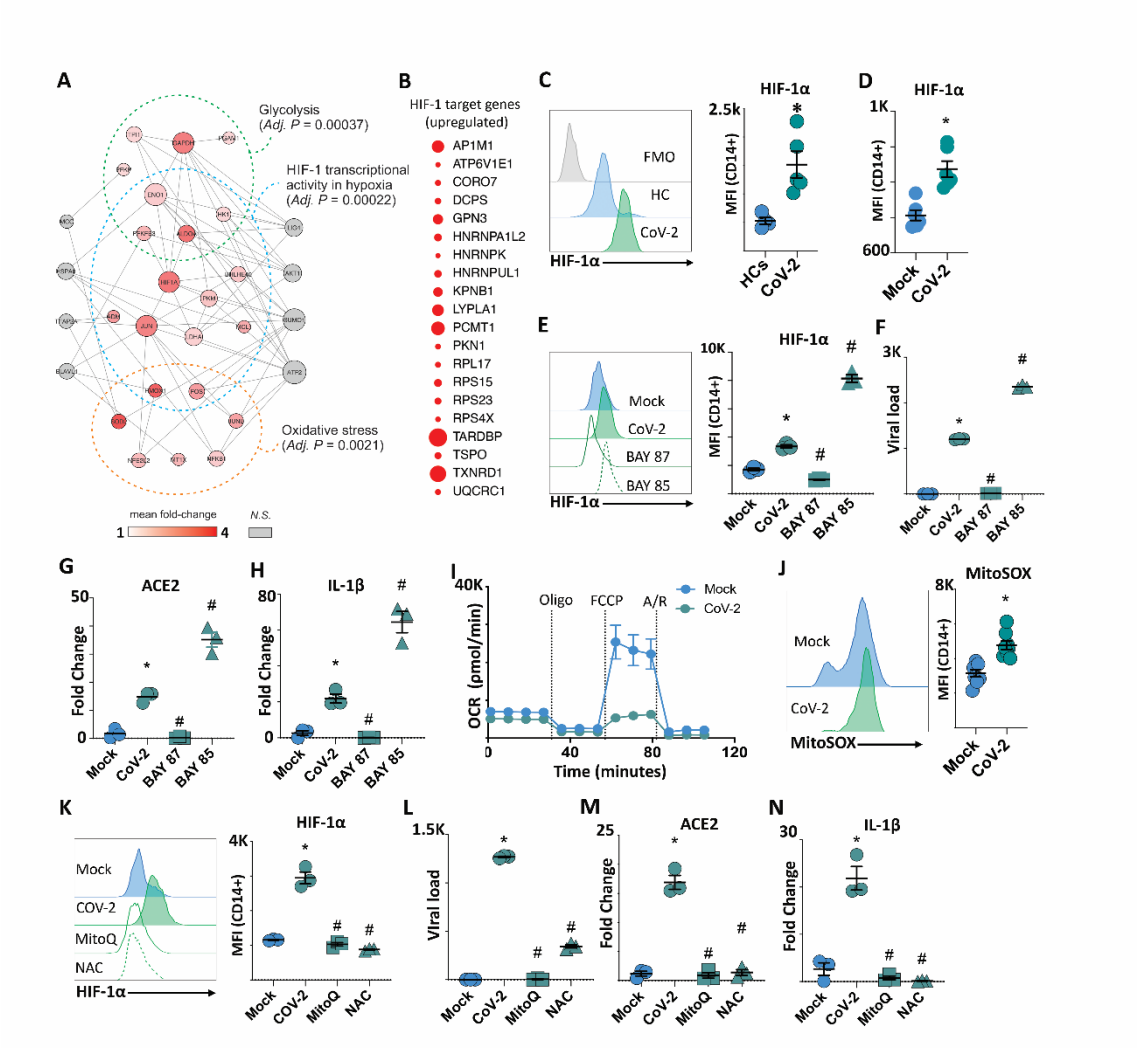

Figure 3. mtROS/HIF-1αa-axis is necessary for SARS-CoV-2 replication in human monocytes.

(A) Single-cell RNAseq data showing enrichment of HIF-1, glycolysis and oxidative stress pathways in SARS-CoV-2 (CoV-2)-infected human monocytes.

(B) Human monocytes were infected with mock control or CoV-2 (MOI 0.1) for 1 h under continuous agitation and incubated for 24 h. Enrichment of HIF-1α target genes in CoV-2-infected monocytes.

(C) Peripheral blood mononuclear cells from healthy controls (HCs) and COVID-19 patients (CoV-2) were stained with CD14 plus HIF-1α and HIF-1α was determined by flow cytometry.

(D) Human monocytes were infected with mock control or CoV-2 (MOI 0.1) for 1 h under continuous agitation and incubated for 24 h. HIF-1α expression was assessed by flow cytometry on $CD14^+$ monocytes.

(E-H) Human monocytes were pre-treated for 2 h with HIF-1α stabilizer BAY85-3934 (BAY85) and inhibitor BAY87-2243 (BAY87) prior to CoV-2 infection (MOI 0.1) for 1 h under continuous agitation. After 24 h, (E) HIF-1α expression was assessed by flow cytometry on $CD14^+$ monocytes and (F) viral load was determined by qPCR. Relative gene expression of

(G) ACE2 and (H) IL-1β in CoV-2 infected human monocytes pre-treated with either vehicle, BAY85 or BAY87.

(I-J) Human monocytes were infected with mock control or CoV-2 (MOI 0.1) for 1 h under continuous agitation. (I) Real-time Oxygen Consumption Rate (OCR) by human monocytes upon mitochondrial stress (MitoStress test: Injections of Oligomycin, FCCP, Rotenone & Antimycin A) 24 h post-infection. (J) Mitochondrial Superoxide (MitoSOX) production was assessed by flow cytometry on $CD14^+$ monocytes 24 h post-infection.

(K-N) Human monocytes were pre-treated for 2 h with antioxidant Mitoquinol (MitoQ) or N-Acetyl Cysteine (NAC) prior to SARS-CoV-2 infection (MOI 0.1) for 1 h under continuous agitation. After 24 h, (K) HIF-1α expression was assessed on $CD14^+$ monocytes and (L) viral load was determined by qPCR. Relative mRNA expression of (M) ACE2 and (N) IL-1β in mock/SARS-CoV-2 infected monocytes pre-treated with either vehicle, MitoQ or NAC.

All data are representative of three independent experiments performed in triplicate. Error bars represent mean ± SEM. *$P < 0.05$ compared to mock. $^{\#}P < 0.05$ compared to CoV-2 (One-Way ANOVA and Tukey post hoc tests).

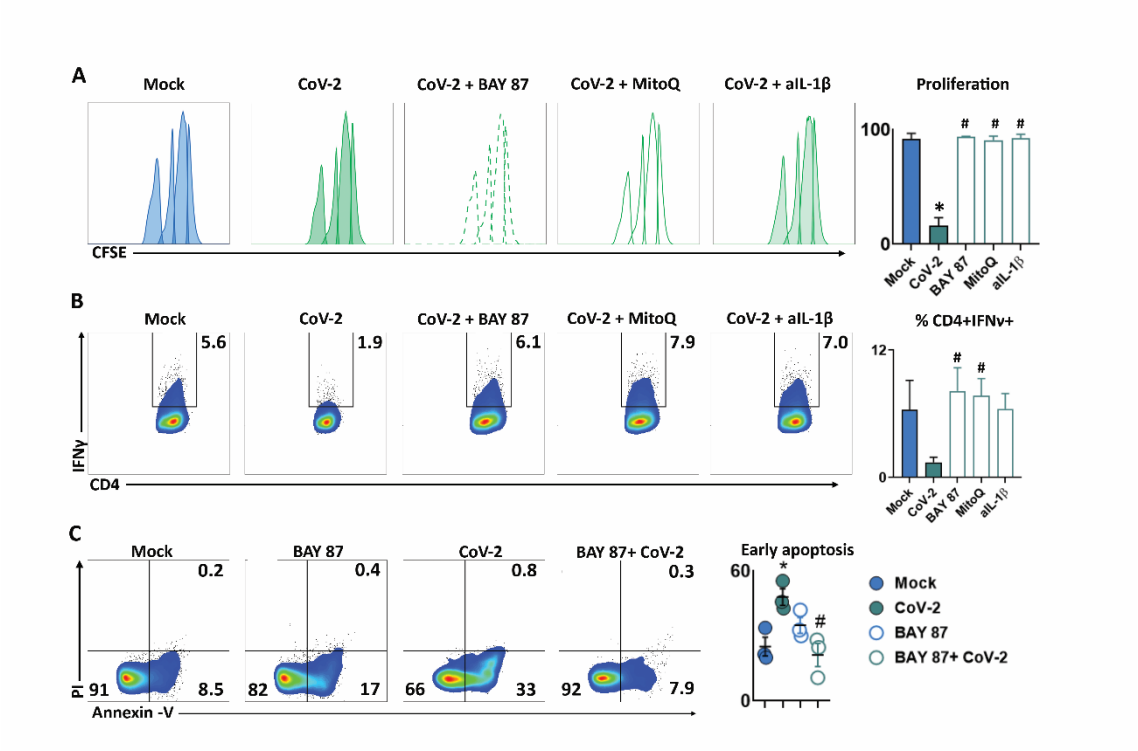

Figure 4. Monocyte metabolism modulates T cell and epithelial cell response to SARS-CoV-2.

(A-B) Human lymphocytes were isolated from peripheral blood, stained with CFSE and cocultured with allogeneic PBMCs for 72 h in the presence of conditioned media from mock or SARS-CoV-2 (CoV-2) monocytes pre-treated with vehicle, BAY87-2243 (BAY87) and Mitoquinol (MitoQ). For the experiment with anti-IL-1β (aIL-1β), lymphocytes were given conditioned media from CoV-2-infected monocytes with aIL-1β. (A) Proliferation and (B) percentage of viable CD4+IFN-γ+ T cells were determined by flow cytometry and showed by representative dot plots. Data represent mean ± SEM of at least three independent experiments performed in triplicate. *P < 0.05 compared to mock. #P < 0.05 compared to CoV-2 (A) One-Way ANOVA and Tukey post hoc tests. (B) Unpaired student's t test CoV-2 versus BAY87 and CoV-2 versus MitoQ.

(C) Human lung epithelial cell line A549 was cultured for 24 h in the presence of conditioned media from mock or CoV-2-infected monocytes pre-treated with vehicle or BAY87. Representative dot plots of cellular apoptosis by Annexin V/PI staining. Data represent mean ± SEM of at least three independent experiments performed in triplicate. *P < 0.05 compared to mock. #P < 0.05 compared to CoV-2 (One-Way ANOVA and Tukey post hoc tests).

SUPPLEMENTAL INFORMATION

Elevated glucose levels favor SARS-CoV-2 infection and monocyte response through a HIF-1α/glycolysis dependent axis

Ana Campos Codo[1,16], Gustavo Gastão Davanzo[1,16], Lauar de Brito Monteiro[1,16], Gabriela Fabiano de Souza[2], Stéfanie Primon Muraro[2], Victor Corasolla Carregari[3], Carlos Alberto Oliveira de Biagi Junior[4], Fernanda Crunfli[3], Jeffersson Leandro Jimenez Restrepo[5], Pedro Henrique Vendramini[3], Guilherme Reis-de-Oliveira[3], Karina Bispo dos Santos[2], Daniel Augusto de Toledo Teixeira[2], Pierina Lorencini Parise[2], Matheus Cavalheiro Martini[2], Rafael Elias Marques Pereira Silva[6], Alexandre Borin[6], Laís Durço Coimbra[6], Vinícius O. Boldrini[2], Natalia S. Brunetti[2], Andre S. Vieira[7], Eli Mansour[8], Raisa G. Ulaf[8], Ana F. Bernardes[8], Thyago A. Nunes[8], Luciana C. Ribeiro[8], Andre Palma[8], Marcus V. Agrela[8], Maria Luiza Moretti[8], Helison R Carmo[9], Andrei C Sposito[9], Fabrício Bíscaro Pereira[10], Licio Augusto Velloso[8,11], Marco Aurélio Ramirez Vinolo[2,12], André Damasio[3,12], José Luiz Proença Módena[2], Robson Francisco Carvalho[13], Marcelo A. Mori[3,11,12], Daniel Martins-de-Souza[3,12,14,15], Helder I Nakaya[5], Alessandro S. Farias[2,12],

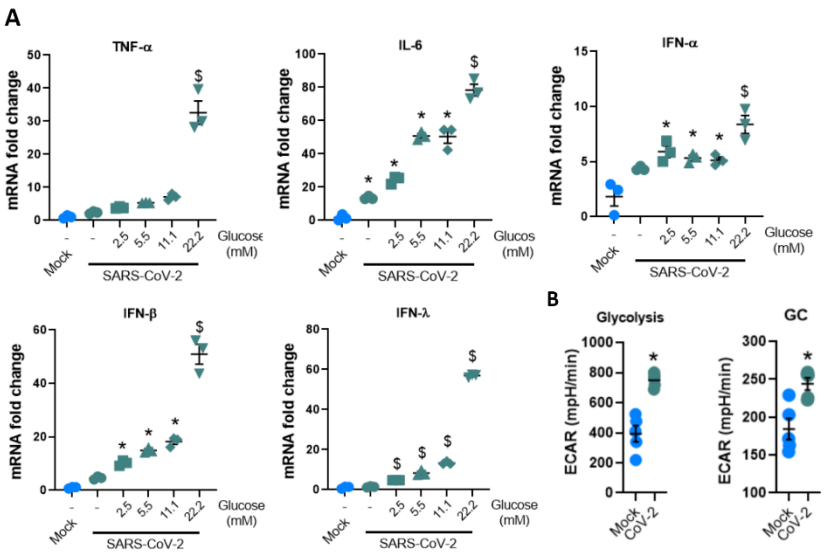

Figure S1. Related to Figure 1. SARS-CoV-2 responds to glucose concentration in extracellular environment.

(A) Human monocytes were infected with mock control or SARS-CoV-2 (CoV-2) (MOI 0.1) for 1 h under continuous agitation and incubated for 24 h in media containing different glucose concentrations (0, 2.5, 5.5, 11.1, 22.2 mM). Relative mRNA expression of cytokines (TNF-α, IL-6, IFN-α, IFN-β and IFN-λ).

(B) ECAR Analysis of Glycolysis (following Glucose injection) and Glycolytic capacity (GC - following Oligomycin injection) in mock control or CoV-2 infected human monocytes.

All data represent mean ± SEM of at least three independent experiments performed in triplicate. *P < 0.05 compared to mock. $P < 0.05 compared to all other groups (One-Way ANOVA and Tukey post hoc tests).

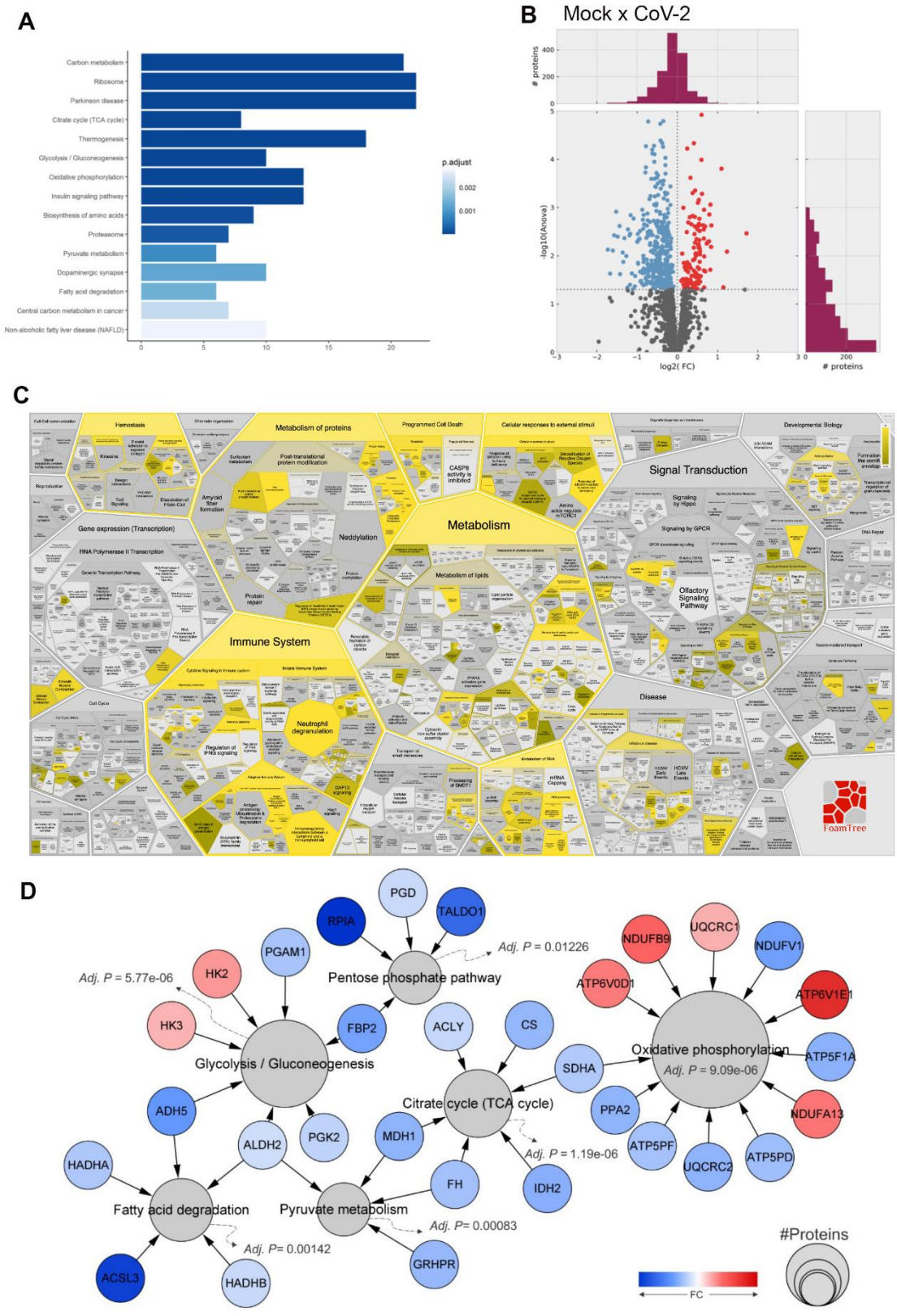

Figure S2. Related to Figure 1 and 3. Proteomic analysis of SARS-CoV-2-infected monocytes.

Human monocytes were infected with mock control or CoV-2 (MOI 0.1) for 1 h under continuous agitation and incubated for 24 h.

(A) Representation of pathways specifically associated with energy metabolism-related protein found differentially expressed.
(B) Volcano plot representing the 1509 quantified proteins, of which 510 were found significantly differentially expressed.
(C) Biological processes associated with the 510 differentially expressed proteins (Reactome).
(D) Differentially expressed proteins associated with the main energy/oxidative pathways.

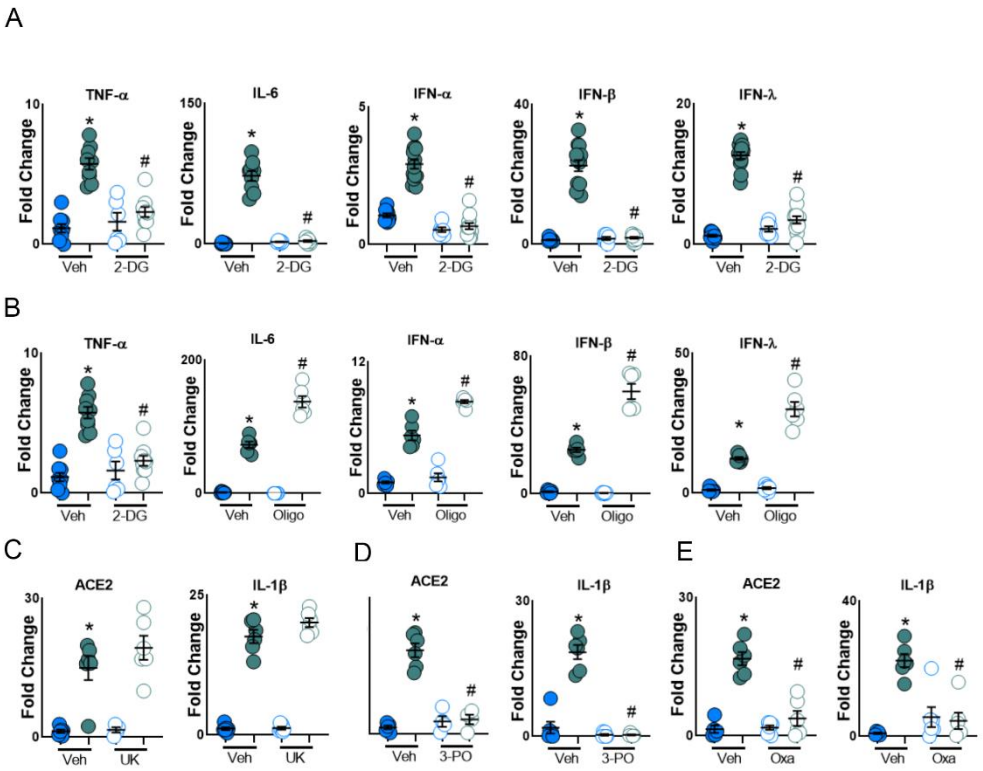

Figure S3. Related to Figure 2. Glycolysis is essential for monocyte inflammatory response to SARS-CoV-2.

Human monocytes were pre-treated with either glycolysis inhibitor 2-DG, PFKFB3 inhibitor 3-PO, LDH-A inhibitor Oxamate (OXA), mitochondrial pyruvate carrier inhibitor UK-5099 (UK) or ATP synthase inhibitor Oligomycin (Oligo) for 2 h prior to SARS-CoV-2 (CoV-2) infection (MOI 0.1) for 1 h under continuous agitation and incubation for 24 h.

(A) Relative mRNA expression of TNF-α, IL-6, IFN-α, IFN-β and IFN-ƛ by qPCR in infected monocytes pre-treated with 2-DG.

(B-E) Relative gene expression ACE2 and IL-1β in infected monocytes pre-treated with (B) 3-PO, (C) Oxamate and (D) UK-5099.

(E) Relative mRNA expression of TNF-α, IL-6, IFN-α, IFN-β and IFN-ƛ by qPCR in infected monocytes pre-treated with Oligomycin.

All data are representative of three independent experiments performed in triplicate. Error bars represent mean ± SEM. *P < 0.05 compared to mock. $^{\#}$P < 0.05 compared to CoV-2 (One-Way ANOVA and Tukey post hoc tests).

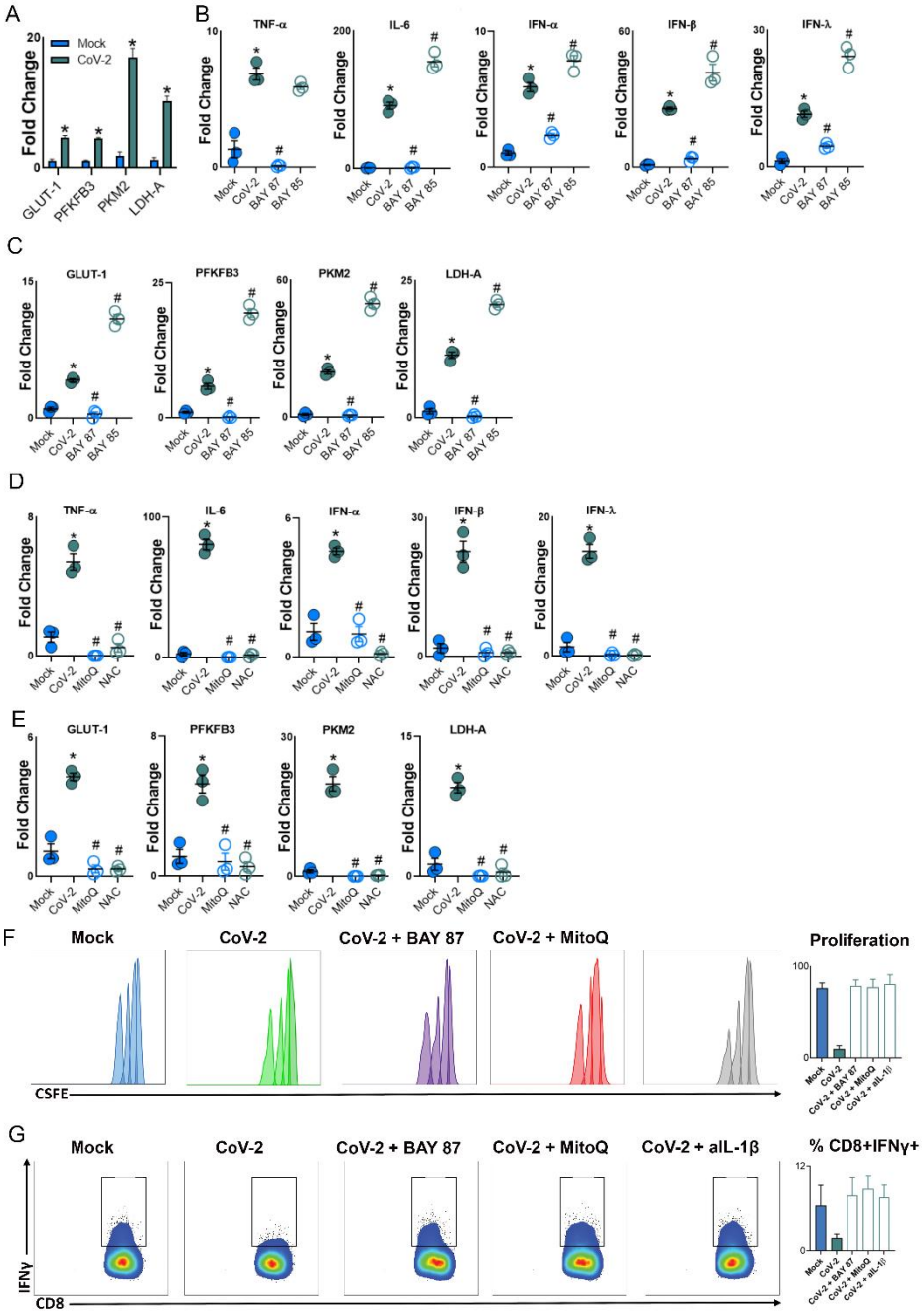

Figure S4. Related to Figure 3 and 4. mtROS/HIF-1α-axis potentiates SARS-CoV-2 induction of glycolytic enzymes and pro-inflammatory cytokines.

(A) Human monocytes were infected with mock control or SARS-CoV-2 (CoV-2) (MOI 0.1) for 1 h under continuous agitation and incubated for 24 h. Relative gene expression of glycolytic enzymes (GLUT-1, PFKFB3, PKM2 and LDH-A).

(B-C) Human monocytes were pre-treated for 2 h with HIF-1α modulators (BAY85 and BAY87) prior to CoV-2 infection (MOI 0.1) for 1 h under continuous agitation and incubation for 24 h. (B) Relative mRNA expression of TNF-α, IL-6, IFN-α, IFN-β, IFN-ƛ, (C) GLUT-1, PFKFB3, PKM2 and LDH-A in monocytes pre-treated with either BAY85 or BAY87.

(D-E) Human monocytes were pre-treated for 2 h with either MitoQ or NAC prior to SARS-CoV-2 infection (MOI 0.1) for 1 h under continuous agitation and incubation for 24 h. (D) Relative gene expression of TNF-α, IL-6, IFN-α, IFN-β, IFN-λ, (E) GLUT-1, PFKFB3, PKM2 and LDH-A in monocytes pre-treated with either MitoQ or NAC.

(F-G) Human lymphocytes were isolated from peripheral blood, stained with CFSE and cocultured with allogeneic PBMCs in the presence of conditioned media from mock or SARS-CoV-2 (CoV-2) monocytes pre-treated with vehicle, BAY87-2243 (BAY87) and Mitoquinol (MitoQ). Lymphocytes were also given conditioned media from CoV-2-infected monocytes with anti-IL-1β (aIL-1β). (F) Proliferation and (G) percentage of viable $CD8^{+}IFN\text{-}\gamma^{+}$ T cells were determined by flow cytometry and are shown by representative dot plots/histograms.

All data are representative of three independent experiments performed in triplicate. Error bars represent mean ± SEM. *P < 0.05 compared to mock. $^{\#}$P < 0.05 compared to CoV-2 (One-Way ANOVA and Tukey post hoc test).

Table S1. General parameters of COVID-19 patients analyzed in this study.

Patient initials	Gender	Age (y)	Admittance O2 saturation (%)
JBJ	M	50	96
JG	M	47	93
EXR	M	47	91
JLS	M	30	84
AEP	M	57	92

*M, male

Table S2. Primer sequences used in qPCR.

Gene	Forward	Reverse
18S	CCCAACTTCTTAGAGGGACAAG	CATCTAAGGGCATCACAGACC
IFN-α	GACTCCATCTTGGCTGTGA	TGATTTCTGCTCTGACAACCT
IFN-*β*	AAACTCATGAGCAGTCTGCA	AGGAGATCTTCAGTTTCGGAGG
IFN-ƛ	ACCTATTTTGTGGCCTATCAGAGCT	CGGCTCCACTTCAAAAAGGTAAT
ACE2	GGACCCAGGAAATGTTCAGA	GGCTGCAGAAAGTGACATGA
GLUT1	CTGCTCATCAACCGCAAC	CTTCTTCTCCCGCATCATCT
LDH-A	AGCCCGATTCCGTTACCT	CACCAGCAACATTCATTCCA
PKM2	ATCGTCCTCACCAAGTCTGG	GAAGATGCCACGGTACAGGT
TNF-α	CCGAGGCAGTCAGATCATCTT	AGCTGCCCCTCAGCTTGA
IL-1β	AAGCTGATGGCCCTAAACAG	AGGTGCATCGTGCACATAAG
IL-6	CCAGCTATGAACTCCTTCTC	GCTTGTTCCTCACATCTCTC
PFKFB3	CAGTTGTGGCCTCCAATATC	GGCTTCATAGCAACTGATCC